ARL-TR-7492 ● SEP 2015

US Army Research Laboratory

Simulating Army-Relevant Spur Gear Contacts with a Ball-on-Disc Tribometer

by Mark R Riggs, Stephen P Berkebile, Adrian A Hood, and Brian D Dykas

NOTICES

Disclaimers

The findings in this report are not to be construed as an official Department of the Army position unless so designated by other authorized documents.

Citation of manufacturer's or trade names does not constitute an official endorsement or approval of the use thereof.

Destroy this report when it is no longer needed. Do not return it to the originator.

ARL-TR-7492 ● SEP 2015

US Army Research Laboratory

Simulating Army-Relevant Spur Gear Contacts with a Ball-on-Disc Tribometer

by Mark R Riggs, Stephen P Berkebile, Adrian A Hood, and Brian D Dykas
Vehicle Technology Directorate, ARL

REPORT DOCUMENTATION PAGE

Form Approved
OMB No. 0704-0188

1. REPORT DATE *(DD-MM-YYYY)*	2. REPORT TYPE	3. DATES COVERED (From - To)
September 2015	Final	14 July 2014–10 August 2015

4. TITLE AND SUBTITLE
Simulating Army-Relevant Spur Gear Contacts with a Ball-on-Disc Tribometer

5a. CONTRACT NUMBER

5b. GRANT NUMBER

5c. PROGRAM ELEMENT NUMBER

6. AUTHOR(S)
Mark R Riggs, Stephen P Berkebile, Adrian A Hood, and Brian D Dykas

5d. PROJECT NUMBER

5e. TASK NUMBER

5f. WORK UNIT NUMBER

7. PERFORMING ORGANIZATION NAME(S) AND ADDRESS(ES)
US Army Research Laboratory
ATTN: RDRL-VTP
Aberdeen Proving Ground, MD 21005-5066

8. PERFORMING ORGANIZATION REPORT NUMBER
ARL-TR-7492

9. SPONSORING/MONITORING AGENCY NAME(S) AND ADDRESS(ES)

10. SPONSOR/MONITOR'S ACRONYM(S)

11. SPONSOR/MONITOR'S REPORT NUMBER(S)

12. DISTRIBUTION/AVAILABILITY STATEMENT
Approved for public release; distribution is unlimited.

13. SUPPLEMENTARY NOTES

14. ABSTRACT
Investigating tribological properties of gear materials, surface finishes, coatings, and lubricants in high-speed and high-load contact conditions is integral to the advancement of drivetrain technology. A focused simulation of gear contacts can be accomplished through a ball-on-disc tribometer with precise control over contact parameters such as the entrainment velocity, slide-to-roll ratio, and contact stress while recording the friction coefficient. These capabilities are integral to studying the functional characteristics of lubricants, materials, and surfaces at the specific contact conditions along a gear tooth profile throughout a meshing cycle. Critical failure conditions can be isolated from the varying contact parameters along the profile of a gear tooth to pinpoint the initiation of failure. To perform this evaluation, the gear contact conditions must be understood and lie within the working envelope of the tribometer. This report outlines the contact conditions commonly experienced in power transmission gearing with an emphasis on military drivetrains and relates them to the operating envelope of a ball-on-disc tribometer.

15. SUBJECT TERMS
gear contacts, spur, WAM, Wedeven Associates, Machine, envelope, ball-on-disc tribometer, simulation

16. SECURITY CLASSIFICATION OF:			17. LIMITATION OF ABSTRACT	18. NUMBER OF PAGES	19a. NAME OF RESPONSIBLE PERSON
a. REPORT	b. ABSTRACT	c. THIS PAGE			Mark R Riggs
Unclassified	Unclassified	Unclassified	UU	44	19b. TELEPHONE NUMBER (Include area code) 410-278-9604

Table of Contents

List of Figures

List of Tables

INTENTIONALLY LEFT BLANK.

1. Introduction

Simulating gear and bearing contacts under the extreme conditions present in high-speed and high-load contacts in aerospace and heavy-duty equipment is attainable with a ball-on-disc tribometer. The ball-on-disc tribometer described within this report is the Wedeven Associates Machine (WAM). The envelope of operation conditions available to the WAM tribometer for parallel surface velocities is presented and projected onto measurement conditions typical of military rotorcraft planetary gear systems. The report begins with a basic description of lubrication and gear fundamentals as a necessary background for the relevance of tribometer testing. Second, gear contact conditions in planetary systems are described. Third, an introduction to the ball-on-disc tribometer and the calculations of contact conditions available to the instrument for parallel surface velocity vectors are given. Finally, discussion and conclusions tie tribometer operation to gear conditions.

2. Lubrication Fundamentals

Lubrication can be divided into several regimes. Hamrock et al.[1] defined 4 regimes: hydrodynamic, elastohydrodynamic, partial/mixed, and boundary. In the early 19th century, Richard Stribeck and Mayo Hersey both observed that the coefficient of friction in conformal contacts followed a universal curve that was a function of the viscosity of the lubricating fluid, speed of the contact, and the inverse of the pressure at the contact.[2] Variants of this Stribeck curve can be used to identify lubrication regimes in both conformal and nonconformal contacts. The general form of the Stribeck curve is shown in Fig. 1. The friction coefficient is highest at low speed, low viscosity, and high load. The opposing surfaces are in physical contact with little liquid lubricant interposed under these conditions. This region is called the boundary lubrication regime because it involves the boundaries of a fluid system coming into contact. Lubrication in this regime may occur through molecular films adsorbed from the lubricant, reacted surface layers, and coatings. The friction coefficient will drop rapidly to a minimum as the speed or viscosity is increased or the load is decreased. Over the range of this drop, the system is in transition from full surface contact in boundary lubrication to fully separated surfaces in elastohydrodynamic lubrication and is therefore called the mixed lubrication regime. Some areas of the surfaces will be separated by a fluid film while others will be in direct contact with each other at surface asperities in mixed lubrication. As speed or viscosity is further increased or load is decreased, the hydrodynamic force of the lubricant is sufficient to fully separate the fluid film. This regime is known as elastohydrodynamic lubrication (EHL). The pressure of

the fluid film in EHL is sufficient to elastically deform the 2 opposing materials in the contact over a relatively large area. The circular contact area of a ball-on-disc tribometer can easily have a radius of 200 μm or more while being separated by a fluid film of a few tens to hundreds of nanometers for the appropriate materials, loads, and geometries used to simulate gear contacts. A representation of this elastic deformation can be seen in the ball as shown in Fig. 2. These contact stresses are discussed further in Section 6. A state of pure hydrodynamic lubrication is achieved when there is no significant elastic deformation of the surface, which occurs at conditions of high speed and viscosity with low load.

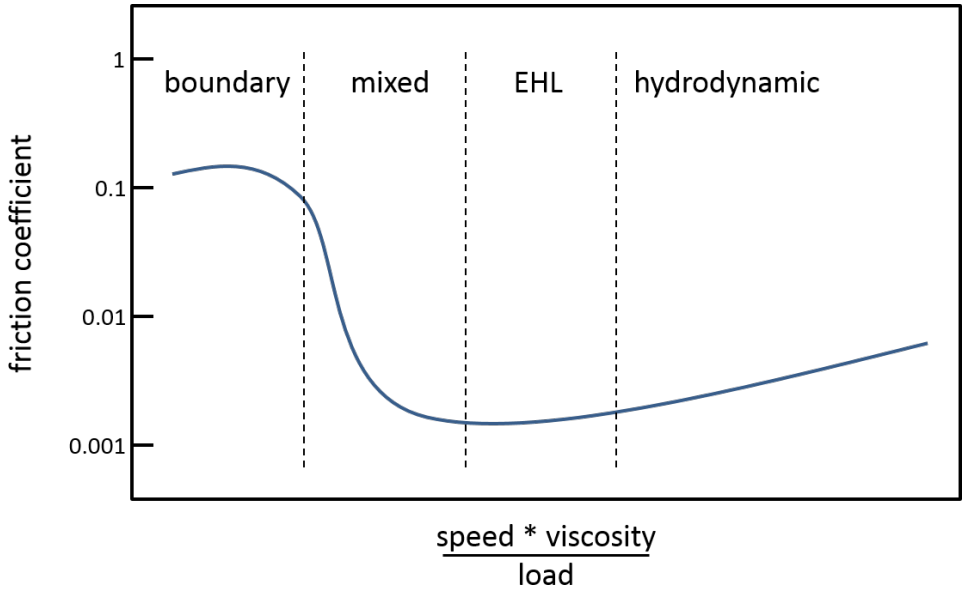

Fig. 1 Generalized Stribeck curve with lubrication regimes labeled

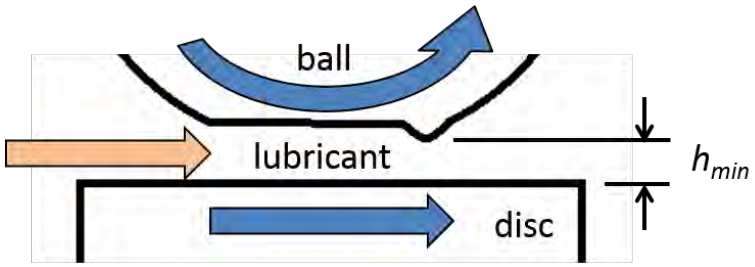

Fig. 2 Typical EHL contact in a ball-on-disc system

Lubrication regimes are primarily distinguished by the film thickness between contacting surfaces and the roughness of those surfaces. The dimensionless film thickness parameter, Λ, helps to characterize the film thickness and predict the

lubrication regime. Λ is shown in Eq.1,

$$\Lambda = \frac{h_{min}}{\sqrt{Ra_1^2 + Ra_2^2}}, \quad (1)$$

where Ra_i is the surface roughness of surface i and h_{min} is the minimum surface separation. The minimum film thickness for elliptical contacts can be estimated by the Hamrock-Dowson equation, which depends on viscosity, speed, and load, among other physical properties of the materials.[1,3] Λ provides a ratio of the fluid film thickness to composite surface roughness and can be used to estimate the severity of asperity contact in the mixed lubrication regime. The mixed lubrication regime ranges from Λ = 1 to 3, and the transition to EHL occurs between Λ = 3 to 4.[4] A representation of a ball and disc separated by a lubricant film in the EHL regime is given in Fig. 2 with the minimum separation, h_{min}, between the surfaces indicated.

Tribological evaluation and experimentation in simplified contacts is used to study lubricants and materials under contact conditions representative of more complex engineering systems. Experiments using simplified contacts help to isolate contact phenomena from system-level interactions, allowing less resource-intensive screening experiments. From a scientific perspective, the greatest advantage of tribological experimentation is the amount of control gained over the tribological contact system and the lack of confounding interactions, which allow specific chemical and physical effects and interdependencies to be isolated from each other. The challenge is to determine the key parameters one must study to achieve relevant results for the questions at hand. Key parameters to consider include temperature, contact stress, surface roughness, environment, load, geometry, wear mechanism, and surface velocities.[5] Restrictions on parameter choice will vary depending on whether the interest is in reproducing a particular contact in a component (more restrictive) or in understanding basic behaviors in a lubricant or material (less restrictive). Compromises will often need to be made to select the important parameters that most faithfully reproduce the phenomena under study because many parameters are mutually dependent.

3. Practical Gear Contact Background

Gears are used to transmit power and change direction, orientation, speed, and torque while maintaining fixed speed ratios. The main types of gears are spur, helical, bevel, spiral bevel, hypoid, and worm. The most widely used are spur gears due to their ease of manufacture as well as their efficiency. Spur gears will be the

focus of this tribology study as points of contact are analyzed for the gear conditions throughout the meshing cycle on the tooth profile. These are relevant to all Army helicopters because spur gears are used in the planetary stages.

3.1 Lubrication

Today's lubricants for high-end military vehicle transmissions meet performance specifications maintained by various branches of the Department of Defense. Lubricants designed to meet these specifications, like most vehicle lubricants, consist of a base stock oil mixed with 1%–20% additives. The base stock is selected for its physical, chemical, and tribological properties[2] and can be a petroleum-derived fluid. However, a synthetic chemical product is often used for its desirable physical properties such as improved stability, temperature capabilities, and tribological properties. A variety of additive chemicals may be used to meet the specification or improve the fluid above specification minimums depending on the application. Additives are added to decrease corrosion, oxidation, friction, deposits, foaming, or wear and to increase load-carrying capacity.

Lubricants for aerospace turbine engines and gearboxes usually meet MIL-PRF-23699[6] and/or MIL-PRF-85734.[7] Although there are few limits set on the composition, most lubricants will use a POE (polyolester) base stock to achieve the stringent requirements imposed by these standards. Both of these specifications require a kinematic viscosity of about 5 cSt at 100 °C. Aerospace lubricants differ from those that meet performance specifications for heavy-duty ground vehicles such as MIL-PRF-2105E,[8] superseded by SAE J2360[9] as of February 2005. The base stock for this specification is required to be derived from petroleum fractions or synthetically prepared compounds, but the highest quality lubricants will typically use fully synthetic PAO (polyalphaolefin) as the base stock. Although lower viscosities are allowable for some grades, ground vehicle viscosities are typically higher than for aerospace lubricants. For example, an 80W-90 grade requires a kinematic viscosity of at least 13.5 cSt.[8]

3.2 Tooth Profile

Almost all of today's parallel axis gears, spur and helical, are based on an involute tooth profile. Figure 3 is a diagram of the meshing region of 2 gears and it is used to define key locations along the tooth face. A key gear parameter is the base radius, as shown in dashed lines. Each gear has a base radius of r_{b1} and r_{b2}, respectively. The outside diameter of each gear is shown with the solid lines of radius of r_{a1} and r_{a2}, respectively.

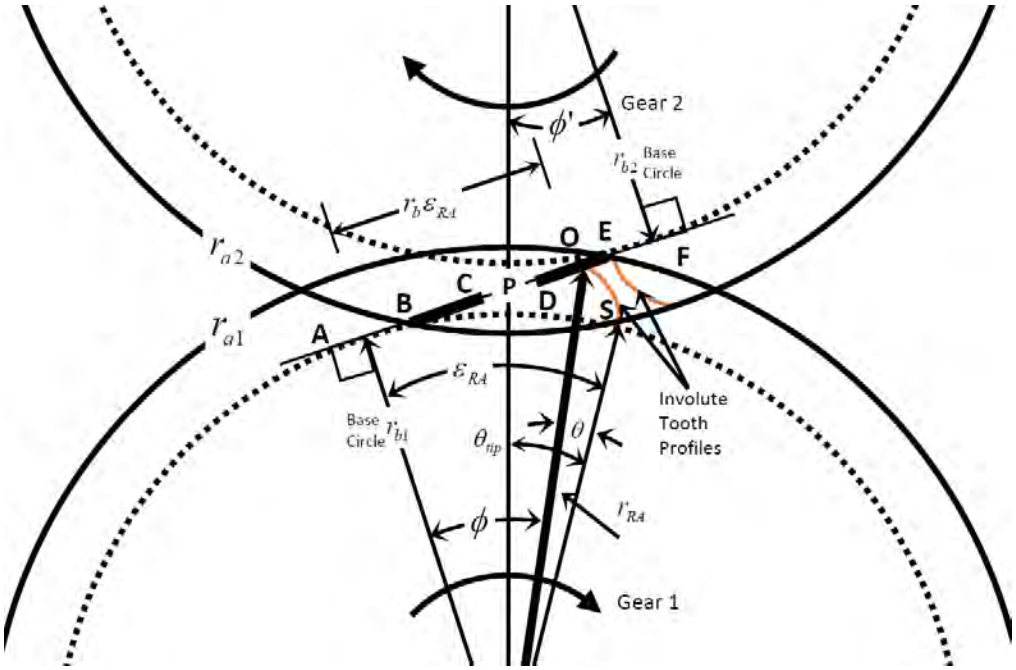

Fig. 3 Gear tooth involute profile locations

The line segment of $\overline{AO}$ is tangent to the base circle of Gear 1 and can be visualized as a string being unwrapped, starting at S and held taut, around a base circle of radius r_{b_1}. The involute tooth profile is the arc $\widehat{SO}$, which represents the path of the imaginary string's tip. The normal to the involute is tangent with the base circle at A. A similar curve can be demonstrated for Gear 2. When 2 meshing involute surfaces come into contact, the mutual normals are tangent to their respective base circles at A and F. This line is referred to as the pressure line or line of action and all tooth contact takes place along this line. Figure 4 shows how points along the pressure line map to positions along the tooth's surface.

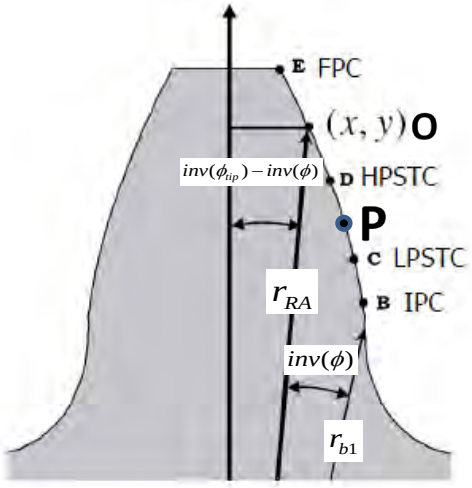

Fig. 4 Mapping of the pressure line to a tooth profile

An arbitrary meshing position (x, y) along the tooth surface and its corresponding position O along the pressure line is given by the load position vector $\vec{r}_{RA}$. The angle ε_{RA}, termed the roll angle, is measured from the start point on the base circle at point *S* and extends to the point of tangency between the tooth profile normal at O and the base circle at point A. The angle ϕ is the instantaneous pressure angle extending from the load position vector to point A and varies with position along the tooth profile. The angle θ is measured from the start of the involute at the base circle and extends to the position vector. By nature of the involute, the length of $\overline{\text{AO}}$ is the arc of the unwrapped portion of the string from the base circle. Therefore, $\overline{AO} = r_b \epsilon_{RA}$ and the following relationship is found:

$$\tan\phi = \frac{r_b \epsilon_{RA}}{r_b} = \epsilon_{RA} = \phi + \theta \, . \tag{2}$$

The angle θ is determined by defining the involute function

$$inv(\phi) \doteq tan(\phi) - \phi = \theta \, . \tag{3}$$

The length of the position vector, r_{RA}, is now given by

$$r_{RA} = \frac{r_b}{cos\phi} \, . \tag{4}$$

Points along the involute are often described in terms of the roll angle, $r_{RA} = tan\,\phi$. The coordinate is given by $x = r_o sin\left(inv(\phi_{tip}) - inv(\phi)\right)$, $y = r_o cos\left(inv(\phi_{tip}) - inv(\phi)\right)$, where $\phi_{tip} = \frac{\pi}{2N} - inv(\phi')$ and ϕ' is the operating pressure angle and represents the angle between the base circle tangent point (A or F) and the centerline. The operating pressure angle depends on the actual distance between gear centers.

The pitch circle is an imaginary circle such that when the 2 gears are mated, their pitch circles are tangent. The point of tangency is termed the pitch point and is denoted as P in Fig. 3. The sum $(r_{p1} + r_{p2}) = CD$ is the center distance between the gear centers. The pressure line $\overline{AF}$ also passes through the pitch point. This geometry produces a stationary pitch point that is the requirement for a pair of gears to maintain a constant velocity ratio, termed conjugate tooth action.

A fundamental condition for 2 gears to properly mesh is that they must share the same base circle pitch. When 2 gears are mated, the following relationship holds:

$$r_{p1} = r_{b1}\cos\phi' = \frac{N_1}{N_2} r_{b_2} cos\,\phi' \ , \tag{5}$$

resulting in

$$\frac{N_1}{2r_{p1}} = \frac{N_2}{2r_{p2}} = DP \, , \tag{6}$$

where DP is termed the diametrical pitch of the gear. Therefore, if standard gears are used, compatibility is ensured if the mating gears share the same DP and pressure angle.

3.3 Determining Key Points along the Pressure Line

This next section derives 5 key meshing locations along a gear's tooth profile. In Fig. 3, Gear 1 is driving Gear 2. The meshing period begins when the tail end of the effective addendum of the driven gear crosses the pressure line, point B. At this point, 2 teeth pairs are in contact, the current one and the previous one. This is characterized by reduced tooth forces due to the load sharing and is the initial point of contact. At point C, the driving gear's previous tooth disengages and the tooth is in single contact mode, characterized by a large increase in load on the current tooth. This position is the lowest point of single tooth contact. This continues until point D at which time the addendum of the driven gear's ensuing tooth passes the pressure line and the gears are in double contact mode again. Point D is termed the highest point of single tooth contact and is significant in that it is usually the point along the tooth that is used to calculate the tooth bending stress.[10] The tooth engagement ends at point E, the final point of contact, when the effective addendum of the driving gear's current tooth passes the pressure line. The line segments along the pressure line are dependent on r_{b1}, r_{b2}, ϕ', r_{a1}, and r_{a2} as well as the amount of backlash. Formulas to calculate key points along the pressure line are given by the equations in Fig. 5.

$$\overline{AF} = (r_{b1} + r_{b2}) \tan \phi' \qquad \overline{BF} = \sqrt{r_{a2}^2 - r_{b2}^2}$$

$$\overline{AB} = \overline{AF} - \overline{BF} \qquad \overline{AE} = \sqrt{r_{a1}^2 - r_{b1}^2}$$

$$\overline{EF} = \overline{AF} - \overline{AE} \qquad \overline{BE} = \overline{BF} - \overline{EF}$$

$$\overline{AP} = r_{b1} \tan(\phi') \qquad \overline{BP} = \overline{AP} - \overline{AB}$$

$$\overline{FP} = r_{b2} \tan(\phi') \qquad \overline{EP} = \overline{FP} - \overline{EF}$$

$$\overline{BD} = \overline{CE} = \overline{AD} - \overline{AB} \qquad \overline{AD} = \overline{AB} + \overline{BD}$$

$$\overline{AC} = \overline{AD} - \overline{CD} \qquad \overline{BD} = \overline{CE} = P_b$$

$$\overline{CD} = 2\overline{P_b} - \overline{BE} \qquad P_b = \frac{2\pi r_b}{N}$$

Fig. 5 Equations to determine key points along the pressure line

The contact ratio, C_r, is a measure of the average number of teeth in contact during a complete rotation. It is given by the ratio of the path of contact length, BE to the base tooth pitch P_b. For most spur gears, $C_r < 2$. Gears with $C_r > 2$ are considered high contact ratio gears and are characterized by smoother and quieter operation. Backlash between teeth must be sufficient to permit free action under the most severe combinations of manufacturing tolerances, alignment errors, and operating temperature variations.[11] An increase in center distance is accompanied by a change in the operating pressure angle due to an increase in the pitch radii. Since the initial contact is delayed due to backlash, the length of the path of contact is shortened, which results in a decrease in the contact ratio. However, the constant speed ratio is unaltered, which is one of the benefits of an involute tooth profile.

3.4 Sliding and Entrainment Velocity

Gear tooth meshing can be separated into 5 stages: engagement, rolling/sliding contact, pure rolling contact, rolling sliding contact, and disengagement. The equations quantifying the sliding velocity, entrainment velocity, and their ratio are derived in the following paragraphs.

The sliding velocity, U_s, is the relative velocity between the meshing surfaces and is defined as $U_s = \left(\overrightarrow{U_1} - \overrightarrow{U_2}\right) \cdot \vec{T}$, where $\vec{T}$ is the tangent vector to the meshing surfaces. The entrainment velocity is the average surface speed in the tangential direction defined as $\frac{1}{2}(\overrightarrow{U_1} + \overrightarrow{U_2}) \cdot \vec{T}$. Figure 6 shows the velocity vectors at an arbitrary position O along the pressure line where $\overrightarrow{U_1} = \overrightarrow{\omega_1} \times \vec{r}_1$, $\overrightarrow{U_2} = \overrightarrow{\omega_2} \times \vec{r}_2$, and the relative velocity $\overrightarrow{U_{12}} = \overrightarrow{U_1}$-$\overrightarrow{U_2}$. Since $\vec{r}_2 = \vec{R} + \vec{r}_1$, $\overrightarrow{U_{12}} = (\overrightarrow{\omega_1} - \overrightarrow{\omega_2}) \times \vec{r}_1 - \overrightarrow{\omega_2} \times \vec{R}$. Due to the nature of meshing gear teeth where the normal direction is known, the tangent vector is given by

$$\vec{T} = \vec{N} \times \vec{k} = \{cos\,\phi'\,\vec{\imath} + sin\,\phi'\,\vec{\jmath}\} \times \vec{k} = sin\,\phi'\,\vec{\imath} - cos\phi'\,\vec{\jmath}, \tag{7}$$

with

$$\overrightarrow{\omega_1}=\omega_1\vec{k} \quad \text{and} \quad \overrightarrow{\omega_2}=-\omega_2\vec{k}\,, \tag{8}$$

$$\vec{r}_1=\overline{PO}\cos\phi'\;\vec{\imath} + (r_{1p} + \overline{PO}\sin\;\phi')\vec{\jmath}\,, \tag{9}$$

and

$$\vec{R} = -CD\vec{\jmath} = -(r_{1p} + r_{2p})\,, \tag{10}$$

results in

$$\overrightarrow{U_{12}} \cdot \vec{T} = \left((\overrightarrow{\omega_1} - \overrightarrow{\omega_2}) \times \vec{r}_1 - \overrightarrow{\omega_2} \times \vec{R}\right) \cdot \vec{T}$$

$$= \left(\begin{vmatrix} i & j & k \\ 0 & 0 & \omega_1 + \omega_2 \\ \overline{PO}\cos\phi' & r_{p1} + \overline{P\,O}\sin\,\phi' & 0 \end{vmatrix} - \begin{vmatrix} i & j & k \\ 0 & 0 & -\omega_2 \\ 0 & -CD & 0 \end{vmatrix} \right) \cdot \vec{T}. \quad (11)$$

$$= -(\omega_1 + \omega_2)\overline{PO} + sin\ \phi' \left[\omega_2 r_{p1} + \omega_2 r_{p2} - \omega_1 r_{p1} - \omega_2 r_{p1}\right].$$

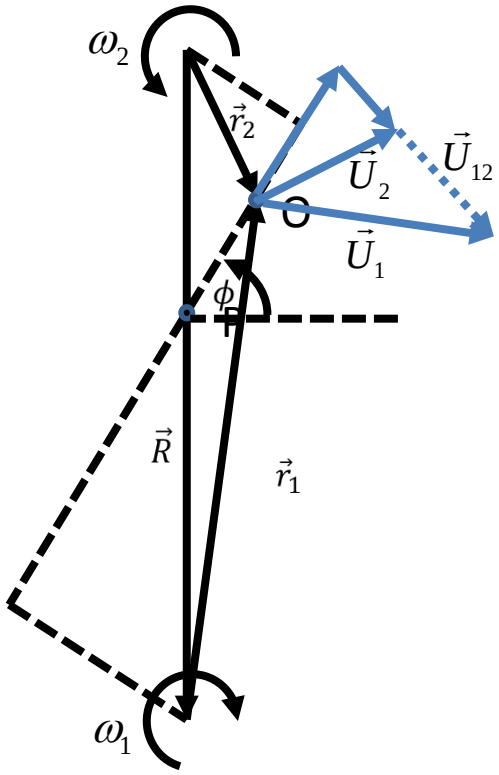

Fig. 6 Gear kinematics representation

Using the relationship $\frac{\omega_2}{\omega_1} = \frac{r_{p1}}{r_{p2}}$, Eq. 11 reduces to

$$U_s = -(\omega_1 + \omega_2)\overline{PO}\,. \quad (12)$$

The entrainment velocity is an average surface velocity in the sliding direction and is given by $U_e = \frac{1}{2}\left(\overrightarrow{U_1} + \overrightarrow{U_2}\right) \cdot \vec{T}$.

$$\tfrac{1}{2}\left(\overrightarrow{U_1} + \overrightarrow{U_2}\right) \cdot \vec{T} = \tfrac{1}{2}\left((\overrightarrow{\omega_1} + \overrightarrow{\omega_2}) \times \vec{r}_1 + \overrightarrow{\omega_2} \times \vec{R}\right) \cdot \vec{T}$$

$$= \tfrac{1}{2}\left(\begin{vmatrix} i & j & k \\ 0 & 0 & \omega_1 - \omega_2 \\ \overline{PO}\cos\phi' & r_{p1} + \overline{P\,O}\sin\,\phi' & 0 \end{vmatrix} + \begin{vmatrix} i & j & k \\ 0 & 0 & -\omega_2 \\ 0 & -CD & 0 \end{vmatrix} \right) \cdot \vec{T}\,. \quad (13)$$

$$= -\tfrac{1}{2}(\omega_1 - \omega_2)\,\overline{PO} - \tfrac{1}{2}\sin\phi'\left[(\omega_1 - \omega_2)r_{p1} + \omega_2 CD\right]$$

Using the relationship $\omega_1 r_{p1} = \omega_2 r_{p2}$, Eq. 13 reduces to

$$U_e = -\frac{1}{2}(\omega_1 - \omega_2)\,\overline{PO} - \omega_1 r_{p1}\sin\phi'\,, \quad (14)$$

which can be further simplified to

$$U_e = -\frac{\omega_1}{2}\left\{\left(1 - \frac{r_{p1}}{r_{p2}}\right)\overline{PO} + 2\overline{AP}\right\}. \tag{15}$$

A table of typical rotorcraft transmission slide velocities, entrainment velocities, and slide-to-roll ratios (SRRs) is given in the Appendix.

3.5 Gear Failure Modes

Gears may fail due to a wide range of mechanisms such as fracture, pitting, and spalling. However, there are a few failure modes directly related to lubrication of the gear and the breakdown of lubricating films. The type of damage that can occur in gears is a function of gear speed and applied load. At low speeds and high loads, excessive wear can occur due to operation in the mixed and boundary lubrication regime when the surfaces are in direct contact. While wear is not a failure mode in itself, it can lead to ending the usefulness of a gear. Beyond standard tribological wear behavior, the main failure modes in gears attributed to lubrication are scoring and scuffing. Both of these failure modes occur on the contact face of the gear tooth when the lubrication is insufficient to keep the meshing surfaces separated. Scoring is a severe form of wear characterized by the formation of extensive grooves and scratches in the direction of sliding[12] and can occur at modest loads but high speeds. Scuffing occurs from the transfer of metal from one surface to another due to localized welding and tearing. Davis[13] reported that oxide layers that normally protect the gear tooth surfaces may be broken through, allowing the bare metal surfaces to weld together. Scuffing often includes plastic flow of material, may involve oxidative wear with sufficient frictional heating, and tends to occur when sliding velocities are high at high loads, at high temperatures, with a lack of extreme pressure additives, or under insufficient lubrication.[14] The increase in temperature through frictional heating can increase the amount of scuffing in a run-away process. Tribological testing that seeks to reproduce gear failure will necessarily need to produce scuffing and scoring events.

3.6 Gear Contact Stress

Typically, contacting spur gears are modeled as 2 cylinders in contact. According to Hertzian contact theory[15]

$$\sigma_{max} = \sqrt{\frac{K_v W_t\left(\frac{1}{R_1}+\frac{1}{R_2}\right)}{\pi l\left(\frac{1-\nu_1^2}{E_1}+\frac{1-\nu_2^2}{E_2}\right)}}, \tag{16}$$

where W_t is the tooth load, l is the facewidth, K_v is a dynamic factor, and $\nu_1, \nu_2, E_1,$ and E_2 are the Poisson's ratios and elastics constants for their respective gears. The variables R_1 and R_2 are the surface radii at the contact point, and from Fig. 3, $R_1 = \overline{AO}$ and $R_2 = \overline{OF}$. At the pitch point, $W_t = \frac{63{,}057 * H}{\omega_1 r_{p1}}$ lb, where H is in horsepower and $\omega_1$is in revolutions per minute. The contact stress for several Army-relevant planetary gear systems has been calculated and reported in Section 8 of this report using these values and methodology. Maximum contact stresses of 1.5 GPa and bending stresses of 0.4 GPa are rarely exceeded in typical helicopters.[16]

4. Ball-on-Disc Tribometer

Ball-on-disc tribometers are an excellent method for studying EHL and mixed lubrication sliding contacts. The WAM shown in Fig. 7 is a ball-on-disc tribometer capable of high speeds and loads with precise control over the contact conditions. The WAM is able to simulate a wide variety of gear and bearing contacts due to the independent control over ball and disc velocities and the versatility of ball-disc positioning. The WAM allows for control over the vertical contact load, oil flow rate, entrainment velocity, slip percentage, specimen temperature, and direction of surface velocity vectors (skew). Tests are run on a specified track diameter defined by the location of the ball and disc contact. The traction coefficient is measured between the ball and disc to study the friction behavior along with temperature measurements and machine instrumentation.

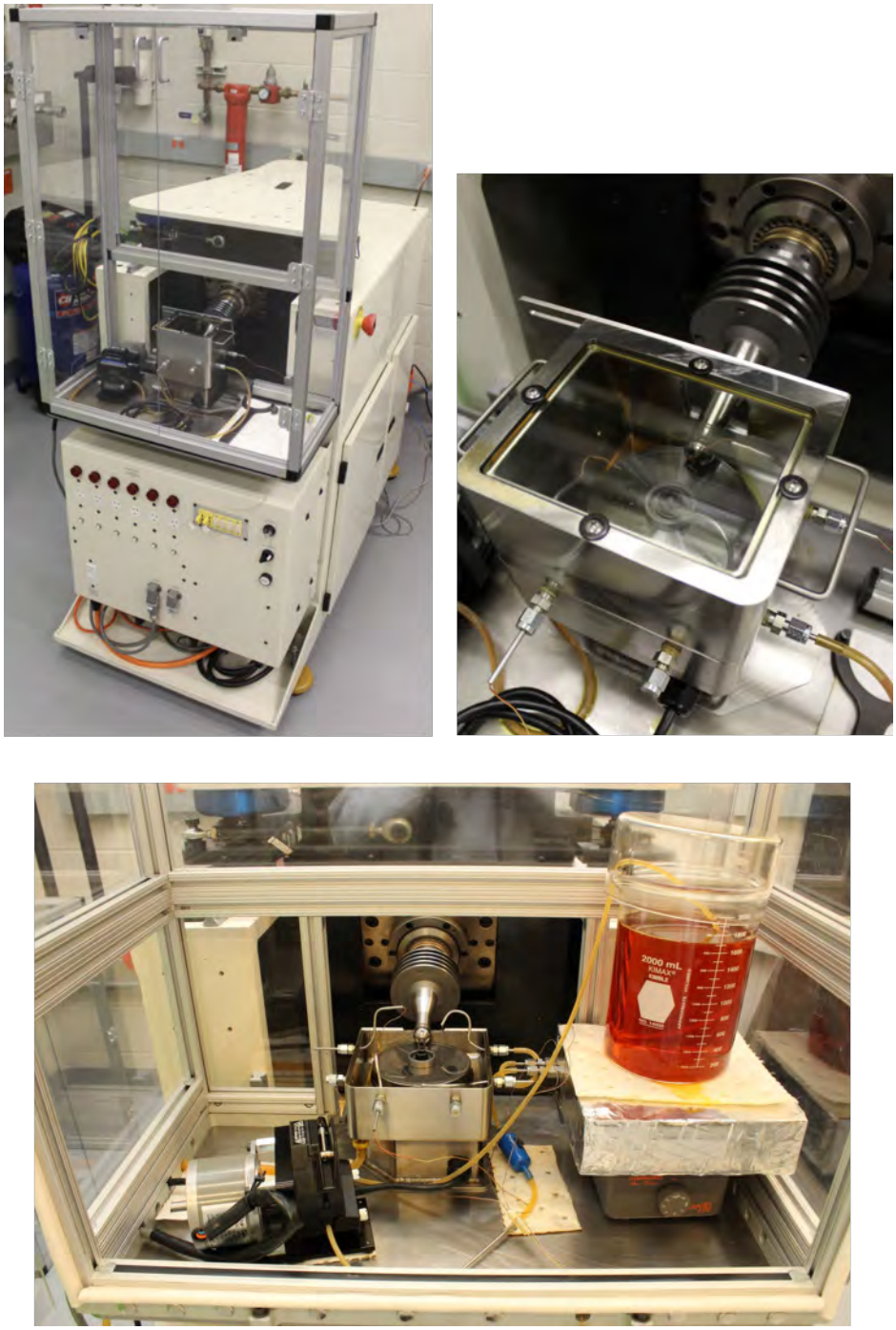

Fig. 7 WAM (model 14) ball-on-disc tribometer

The WAM provides information on lubricant properties, material properties, and failure modes. The primary experimental output of the WAM is the friction coefficient; however, the WAM is also well suited to the study of nonfatigue failure mechanisms such as wear, scuffing, and coatings fracture. Beyond tribological parameters causing failure and time to failure, the ball and disc track surfaces can

be inspected after 1) experimentation to characterize the effect of particular contact conditions in terms of morphological and chemical changes and 2) determination of wear mechanisms and severity. A variety of materials and lubricants can be evaluated under particular contact conditions of interest. Materials may be either coated or uncoated as long as they are able to be machined into the ball and disc specimen size and have the mechanical strength to withstand the contact. The effects of extrinsic properties such as roughness or temperature can also be evaluated in how they affect friction coefficient and types of failure.

5. WAM Speed Capabilities

The ball and disc motors are independent and bidirectional to give a wide range of operating conditions. The ball spindle is capable of rotating up to 16,000 rpm in a clockwise (positive) or counterclockwise (negative) direction. The disc spindle is also capable of rotating in both directions up to a maximum speed of 12,000 rpm. The rotational velocities correspond to linear surface velocities as shown in Fig. 8. The linear velocities for the ball and disc are shown in Eqs. 17 and 18.

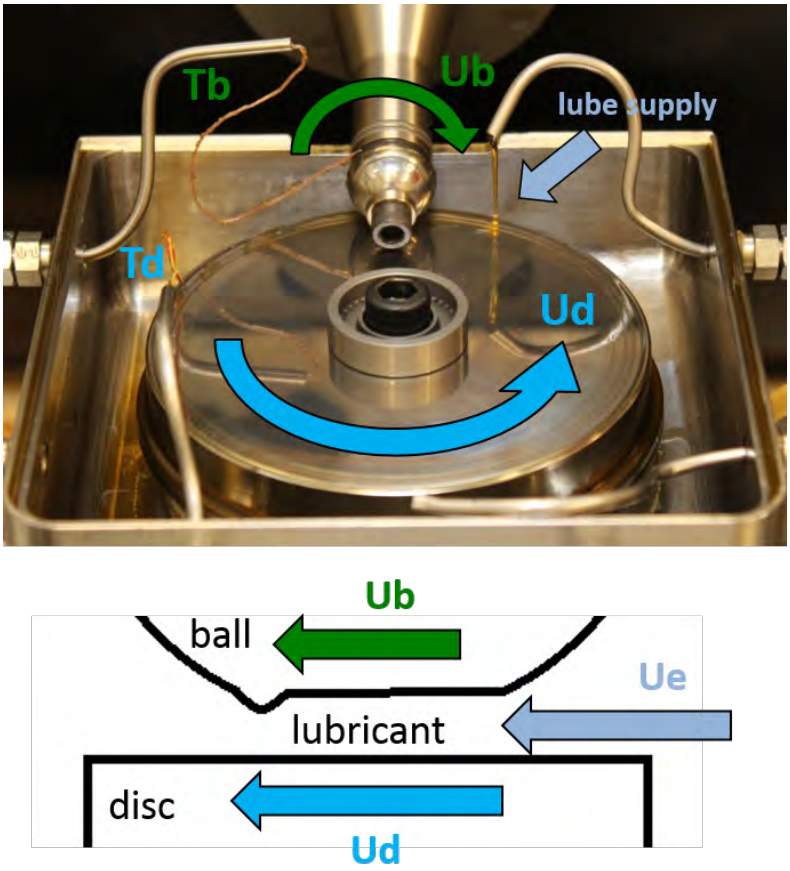

Fig. 8 WAM Detail of typical velocities, temperatures, and oil application

$$U_b = \frac{\pi * Ball\ Speed\ (RPM) * Ball\ Diameter(m)}{60} = Ball\ Velocity\ \left(\frac{m}{s}\right). \quad (17)$$

$$U_d = \frac{\pi * Disk\ Speed\ (RPM) * Track\ Diameter(m)}{60} = Disk\ Velocity\ \left(\frac{m}{s}\right). \quad (18)$$

The entrainment velocity is an average of the ball linear velocity and the disc linear velocity as shown in Eq. 19. The entrainment velocity corresponds to the linear velocity of a gear tooth at its pitch diameter.

$$U_e = \frac{U_b + U_d}{2} = Entrainment\ Velocity\ \left(\frac{m}{s}\right). \quad (19)$$

The sliding velocity is the relative velocity between the 2 contacting surfaces and calculated from the ball velocity less disc velocity as shown in Eq. 20. The slip percentage is the sliding velocity divided by the entrainment velocity and is often given as the SRR. The slip percentage and the SSR are given in Eqs. 21 and 22.

$$U_s = U_b - U_d = Sliding\ Velocity\ \left(\frac{m}{s}\right). \quad (20)$$

$$\frac{U_s}{U_e} * 100\% = Slip\ Percentage\ (\%). \quad (21)$$

$$\frac{U_s}{U_e} = SRR\ (Slide\ to\ Roll\ Ratio). \quad (22)$$

The ball and disc radii contribute toward ranges of capable entrainment velocities. The standard disc size is 109.7 mm with a recommended maximum safe track diameter of 103 mm and a minimum recommended safe track diameter of 67 mm. The ball is typically 20.64 mm in diameter, but the ball spindle adjusts its angle to give the correct point of contact on the disc. This ball-spindle angle, needed to give the correct track diameter, changes the effective ball diameter at the point of contact. The effective ball diameter is given in Eq. 23, where θ is the ball spindle angle from horizontal in degrees. The maximum track diameter of 103 mm has a corresponding spindle angle of 11.4° while the minimum track diameter of 67 mm has an angle of 17.6°. The effect of changing the ball and disc diameters gives a maximum entrainment speed of 40.8 m/s and 29.3 m/s for the maximum and minimum track diameters, respectively.

$$bd_e = \cos(\theta) * bd = effective\ ball\ diameter\ (m). \quad (23)$$

To simulate gear contacts, the researcher will often want to simulate a given entrainment velocity and corresponding slip percentage. It is good practice to ensure the parameters are within the maximum and minimum ball and disc speeds during the test research plan formulation. Equation 24 is used to convert the entrainment velocity and slip percentage into a ball speed and rpm, and Eq. 25 uses the calculated ball speed and given entrainment velocity to back out the disc speed

in rpm. Equations 24 and 25 assume linear ball and disc velocities in the same direction, perpendicular to the ball spindle. The required parameters are given in Table 1.

$$bs = \frac{300*sp*U_e+60{,}000*U_e}{bd_e*\pi}. \tag{24}$$

$$ds = \frac{120{,}000*U_e-bs*bd_e*\pi}{\pi*td}. \tag{25}$$

Table 1 Parameters and units

Variable	Units	Description
bs	rpm	Ball speed
ds	rpm	Disc speed
td	mm	Track diameter
bd_e	mm	Effective ball diameter
sp	%	Slip percentage

The reverse calculations can be done with Eqs. 26 and 27.

$$U_e = \frac{\pi}{120{,}000}(ds * td + bs * bd_e). \tag{26}$$

$$Slip = 200\left(\frac{bs*bd_e-ds*td}{ds*td+bs*bd_e}\right). \tag{27}$$

The speed operating envelope is the range of possible entrainment velocities and slip percentages capable of being produced by the WAM for parallel surface velocities. The parameters used to solve for the WAM envelope at the maximum and minimum track diameters are shown in Table 2. All possible combinations of ball and disc speeds that do not exceed the physical limitations of the machine have been calculated with a spacing of 100 and 75 rpm for the ball and disc, respectively, using the maximum track diameter. The result of this calculation is shown in Fig. 9 translated into entrainment velocity and slip percentage. This map of points indicates that there are well-defined curves bounding the WAM envelope.

Table 2 WAM operating envelope physical parameters

Characteristic	Parameter	Max	Min	Units
Spindle speeds	Ball	16,000	–16,000	rpm
	Disc	12,000	–12,000	rpm
Test diameters	Ball – effective	20.2	19.7	mm
	Disc	103	67	mm

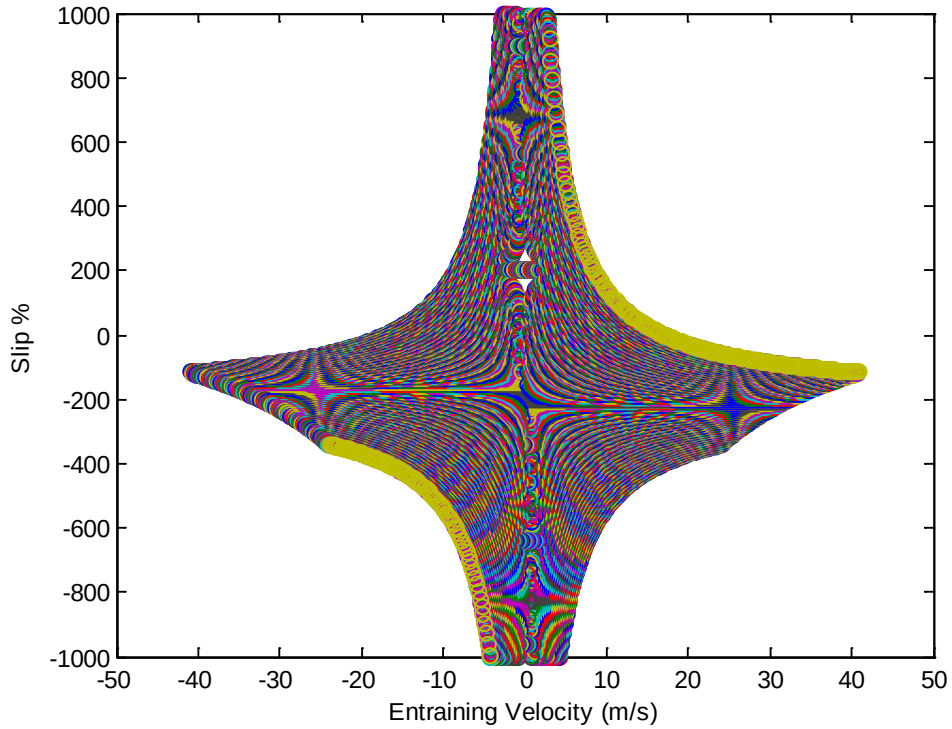

Fig. 9 WAM operating envelope for maximum track diameter

The 4 boundaries are the maximum or minimum speed for each spindle across the opposite spindle's speed range. The first boundary is traced by the disc spindle speed range with the ball spindle held at its minimum speed. The second boundary is also traced by the disc spindle, but the ball is held at its maximum speed. The third and fourth boundaries follow the same pattern with the disc spindle held constant at its minimum and maximum speeds, respectively.

The equations for these boundaries in the form of slip as a function of entrainment velocity can be derived from Eqs. 25 and 26 while holding all values constant with one varying parameter to trace the curve. The equations for each boundary take a similar form with different constants, as shown in Eq. 28 with the constants defined in Table 3. Table 4 gives the numerical values for the constants with a maximum track diameter.

$$Slip\ \% = \frac{A+B*U_e}{C*U_e}\,. \tag{28}$$

Table 3 Coefficients in variable form

Boundary No.	Ball Speed (rpm) $\times 10^3$	Disc Speed (rpm) $\times * 10^3$	A	B	C
1	Bs_{min}	$Ds_{min}\ to\ Ds_{max}$	$400bs \times bd_e$	$\frac{-2.4 \times 10^7}{\pi}$	$\frac{120{,}000}{\pi}$
2	Bs_{max}		$-400bs \times bd_e$		
3	$Bs_{min}\ to\ Bs_{max}$	Ds_{min}	$400ds \times td$	$\frac{2.4 \times 10^7}{\pi}$	
4		Ds_{max}	$-400ds \times td$		

Table 4 Coefficient values (maximum track diameter)

Boundary No.	Ball Speed (rpm) $\times 10^3$	Disc Speed (rpm) $\times 10^3$	$A \times 10^8$	$B \times 10^6$	$C \times 10^4$
1	–16	–12 to 12	–1.2948	–7.6394	3.8197
2	16		1.2948		
3	–16 to 16	–12	4.944	7.6394	
4		12	–4.944		

The WAM envelope boundary equations for the maximum track diameter are plotted on the entire range of –50 to 50 m/s entraining velocity in Fig. 10. The WAM envelope is shaded and outlined in bold while the remaining portion of the equation is plotted in a thinner line for illustration. The equivalent plot for the minimum track diameter is shown in Fig. 11. The boundary intersections are given in Table 5 for the maximum and minimum track diameters.

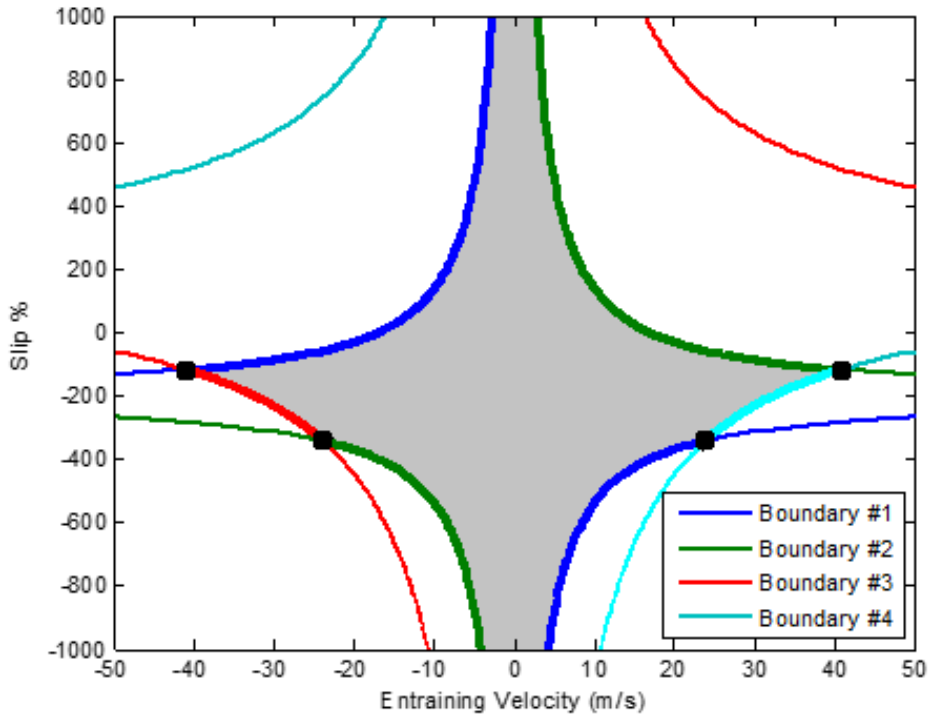

Fig. 10 WAM envelope boundaries for maximum track diameter

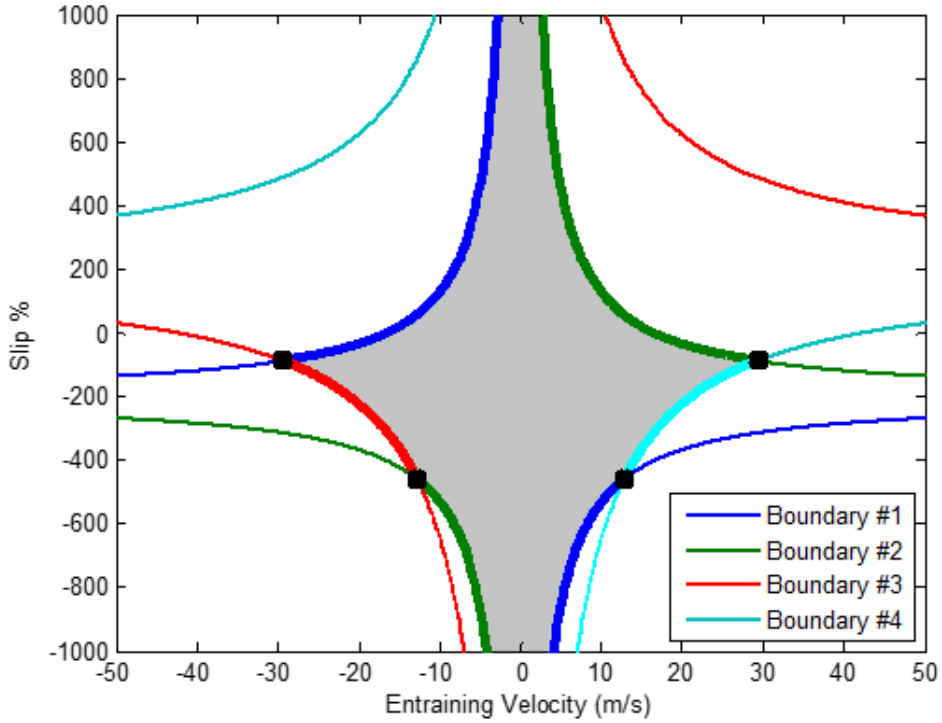

Fig. 11 WAM operating envelope for minimum track diameter

Table 5 WAM envelope boundary intersections

Boundary Intersection	Maximum Track Diameter (103 mm)		Minimum Track Diameter (67 mm)	
	Entrainment Velocity (m/s)	Slip Percentage (%)	Entrainment Velocity (m/s)	Slip Percentage (%)
1 and 3	–40.8	–117	–29.3	–87.4
2 and 3	–23.9	–342	–12.8	–458
1 and 4	23.9	–342	12.8	458
2 and 4	40.8	–117	29.3	87.4

Equation 28 and Table 3 show the first and second boundaries are dependent on the maximum and minimum ball speed and the effective ball diameter. The maximum and minimum ball speed does not change because it is defined as the rotational velocity in revolutions per minute and the effective ball diameter only changes 2.5% based on the ball spindle angle to create pure rolling in the track diameter. This small change leads to the first and second boundaries nearly overlapping when they are plotted together in Fig. 12. The third and fourth boundaries are dependent on the disc speed and track diameter. There is a 35% change in track diameter from 103 to 67 mm. This leads to a significantly larger impact on the third and fourth boundaries, which shrinks the WAM envelope as shown in Fig. 12. Thus, test plans must be formed around the working envelope for the minimum track diameter to run at every available track on the disc.

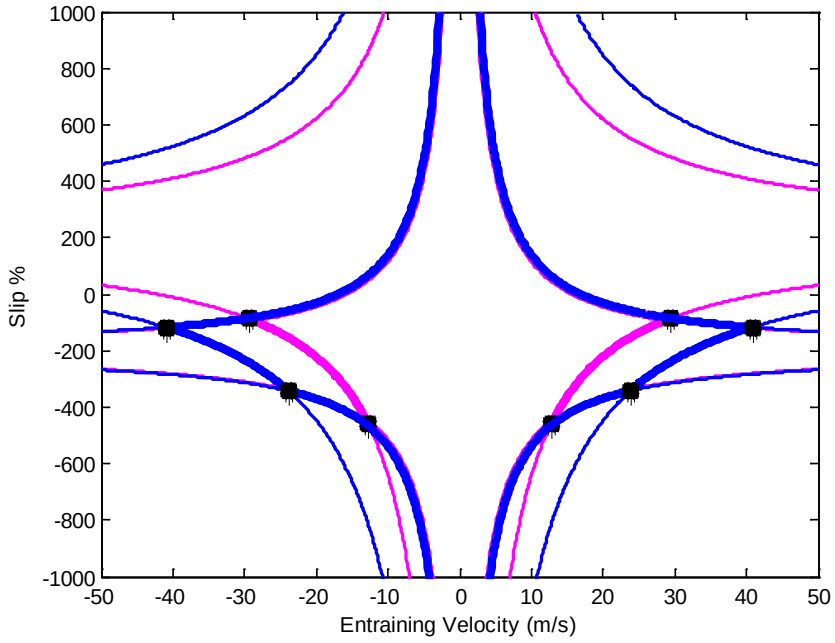

Fig. 12 Comparison of maximum and minimum track diameters

6. WAM Contact Stresses

Loading between the ball and disc represents the Hertzian contact stress caused by torque transmission in a gear pair. The loading capabilities of the WAM are from 0 to 1,200 N, which corresponds to 0–2.79 GPa of stress for an American Iron and Steel Institute (AISI) 9310 contact pair, as calculated by Eqs. 29 and 30, for a flat disc and a ball with a radius of 20.7 mm. The contact stress increases when a ceramic is introduced to the contact pair because of its higher Young's modulus as shown in Table 6. The contact pairs for steel on steel, ceramic on steel and ceramic on ceramic are shown in Figs. 13–15 with the Hertzian contact stress, contact radius, and contact area as a function of load.

$$a = \sqrt[3]{\frac{3F}{8} * \left(\frac{\left(\frac{1-\nu_1^2}{E_1} + \frac{1-\nu_2^2}{E_2} \right)}{\frac{1}{2R_1} + \frac{1}{2R_2}} \right)} \quad . \tag{29}$$

$$P_{max} = \frac{3F}{2\pi a^2} \quad . \tag{30}$$

Table 6 Material properties for Hertzian stress

Material	Young's Modulus (GPa)	Poisson's Ratio
M50	200	0.285
9310	200	0.29
52100	200	0.285
SiN	310	0.3

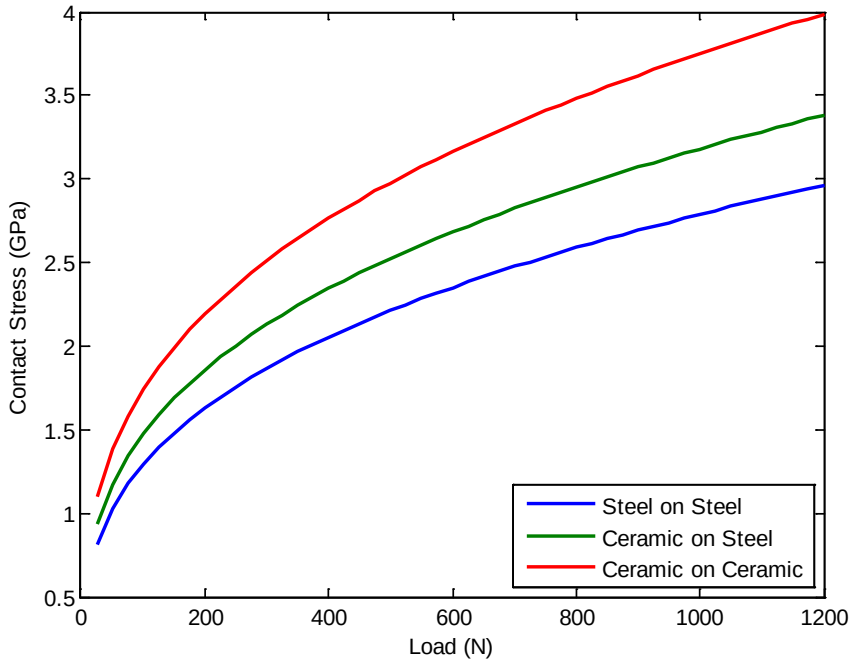

Fig. 13 Hertzian contact stress for steel and ceramic contacts

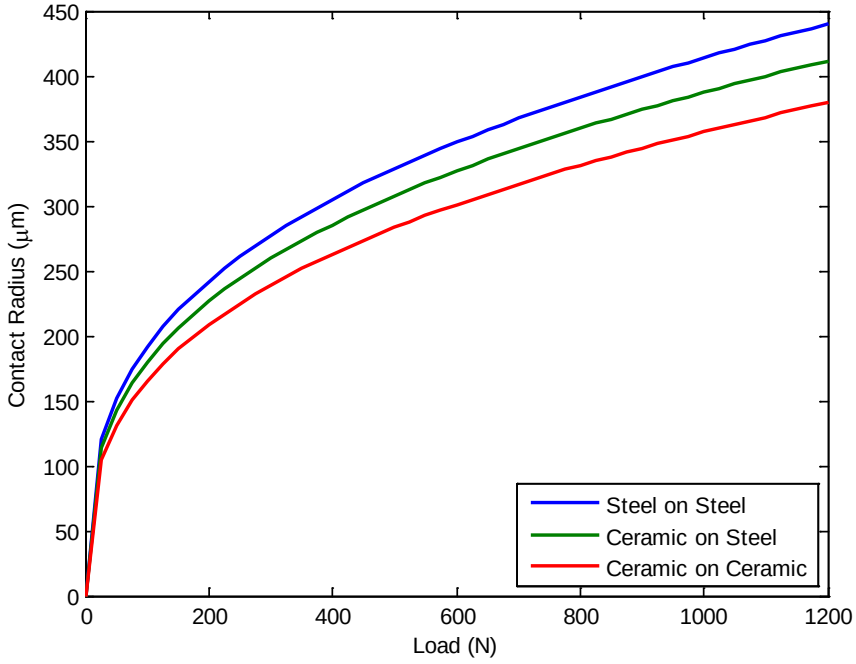

Fig. 14 Contact radius for steel and ceramic contacts

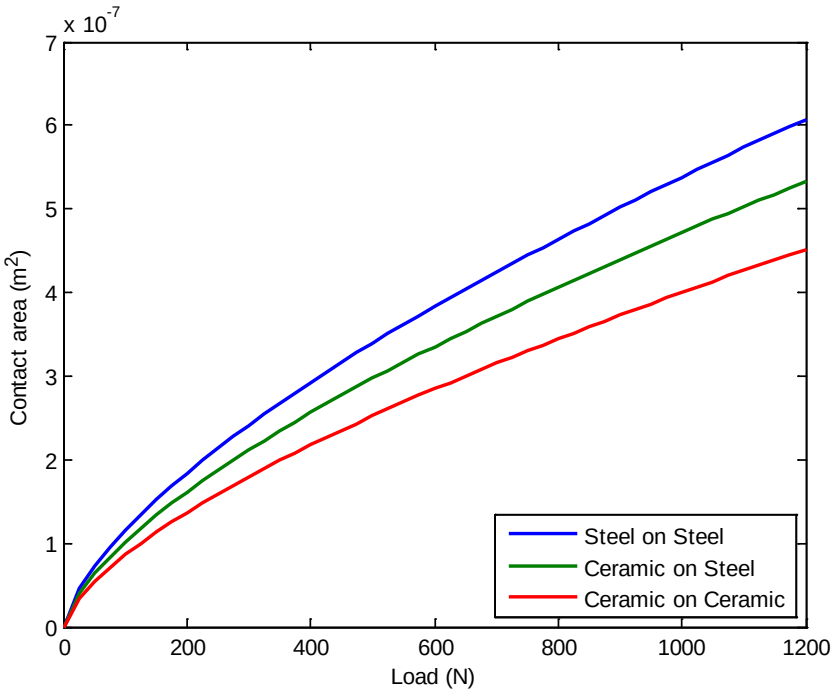

Fig. 15 Contact area for steel and ceramic contacts

7. WAM Specimen Roughness

The surface roughness is an important factor to consider in tribological evaluation. A typical roughness often given for gears is 20 µin, or about 500 nm, although particular applications may require a finer finish. Superfinishing processes that can reduce surface roughness to less than 50 nm are increasing in popularity and use for gear applications. Gears also have a direction to their roughness features from grinding. For spur gears, grinding results in ridges perpendicular to the direction of motion on their teeth. The orientation of grinding ridges has been shown to be significant to EHL contacts[17] and should be simulated for tribological evaluation to have the most fidelity. Disc specimens can be ground radially or circumferentially so that the grinding ridges are perpendicular or parallel, respectively, to the direction of surface motion at the contact.

During operation in the boundary, mixed, and EHL regimes, the actual roughness will depend on the contact history from a mild form of wear called run in. The amount of run in depends on time, load, velocities, and surface chemistry. During the run in period, the highest surface asperities are polished off during initial operation, after which little change is seen while operating in the EHL and upper mixed regime. Run in has the effect of extending the EHL and mixed lubrication regimes towards lower entrainment velocities as surface roughness is reduced. The

amount of run in is a parameter that must be considered when simulating gear or bearing contacts, and can even be the object of an investigation.

The roughness of a surface affects the lubrication regime, as discussed previously in the Section 2, and is therefore important to reproduce in the ball and disc specimens if a particular application is to be simulated. If the actual surface roughness cannot be reproduced for a particular contact, effort should be given to maintaining a similar lubrication regime by operating at a similar Λ ratio. As mentioned before, Λ ratio depends on the surface roughness and the minimum film thickness h_{min}. In Fig. 16, the minimum film thickness for several viscosities are given over a range of entrainment velocities, while in Fig. 17, the Λ ratio as a function of entrainment velocity is shown for several values of composite surface roughness. The minimum film thickness h_{min} was calculated for both figures from the Hamrock-Dowson equation using a density of 0.9 g/mL, a pressure-viscosity coefficient of 1×10^{-8} m^2/N, a load of 200 N, the material properties for AISI 9310 steel, and the standard WAM specimen sizes given in the previous section.

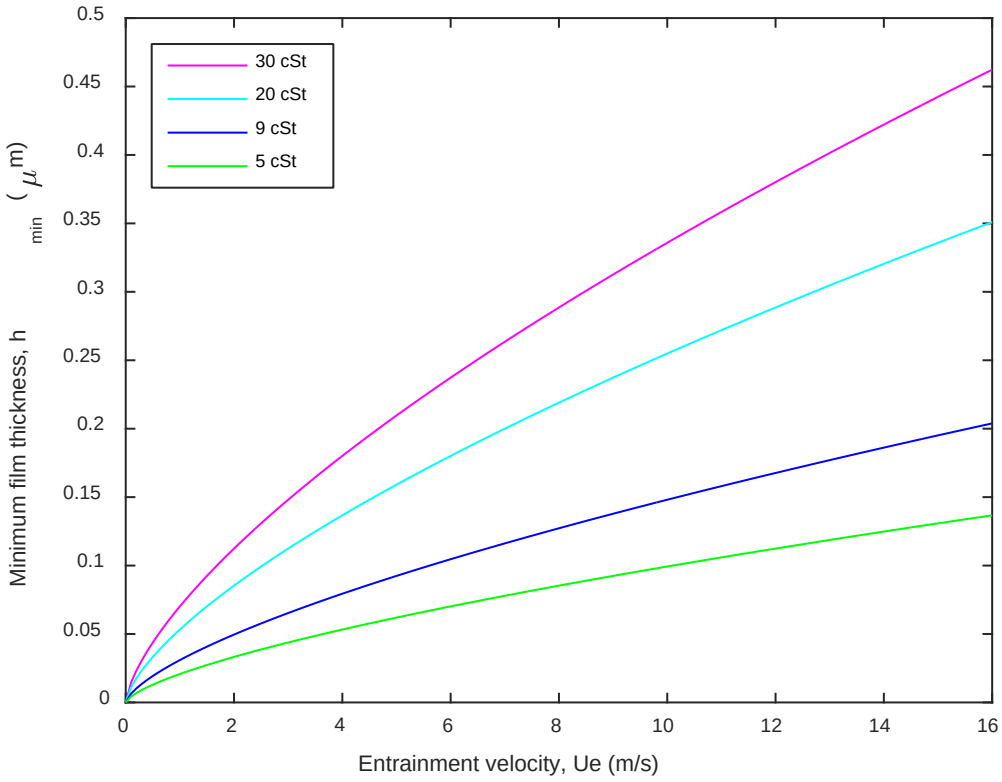

Fig. 16 Minimum film thickness for different lubricant viscosities

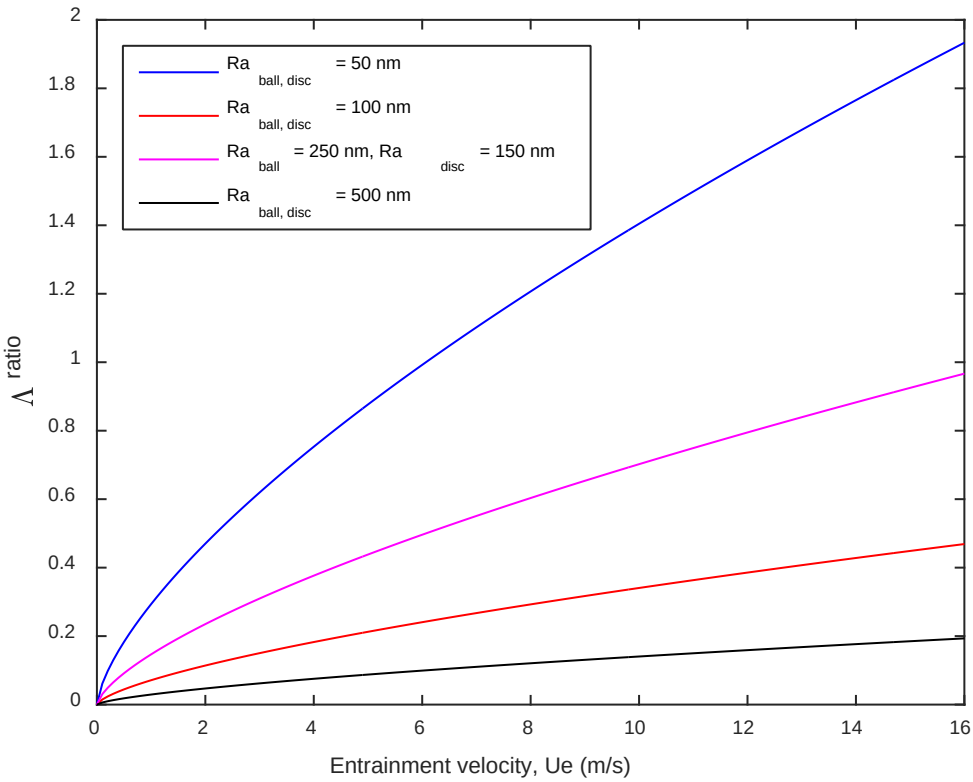

Fig. 17 The Λ ratio for various surface roughnesses with 5-cSt lubricant

8. WAM Envelope versus Army Gear Conditions

The WAM envelope represents the full gamut of operating conditions available for analysis under tribological investigation to simulate Army gear contact conditions. The spur gear applications to be studied have a wide range of entrainment velocities, sliding velocities, and SRRs that were calculated for the CH-47, UH-60, AH-64, and OH-58D using the gear geometry[18] and equations derived previously in Section 3. Their resulting entrainment velocities, slip percentages, and contact stresses are shown in Table 7. Figure 18 shows the Army helicopter values from Table 7 plotted on the WAM operating speed envelope. It can be seen from Fig. 19 that 2 values do not fall within the WAM operating envelope, point B for both the CH-47 lower stage and the NASA test spur gears. While point B, the positive slip extreme condition, does not fit within the WAM envelope for all of the gear sets, it can be simulated with the WAM by simply changing the sign of the slip percentage to fall back within the WAM envelope. Changing the sign of the slip percentage will properly simulate the gear contact because the relative speed between the contacting surfaces is identical. In addition to simulating the speed, the WAM is

able to simulate the contact stresses with a range of 0–2.79 GPa for a steel-on-steel contact conditions. This range fully encompasses the contact stresses described in Table 7, which have a typical value of about 1.3 GPa.

Table 7 Army helicopter spur gear contact conditions

Gear Contacts	Entrainment Velocity (m/s)		Slip Percentage (%)		Contact Stress (GPa)
Location on gear profile	B	E	B	E	P
CH-47 sun/planet lower stage	13.8	12.5	52.5	–65.5	1.30
CH-47 sun/planet upper stage	3.81	4.02	55.2	–52.8	1.30
UH-60	4.42	4.21	33.9	–35.2	1.09
AH-64	4.10	4.13	41.9	–40.9	1.33
OH-58D	2.88	2.66	48.0	–73.3	1.35
NASA test spur gears	15.9	15.9	101	–101	1.29

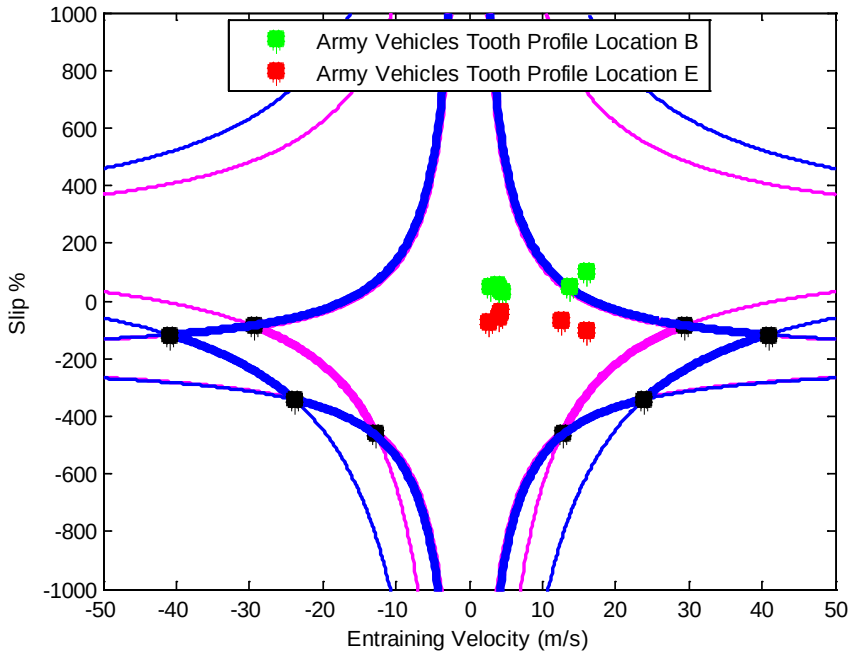

Fig. 18 Army helicopter contact speeds vs. WAM speed envelope

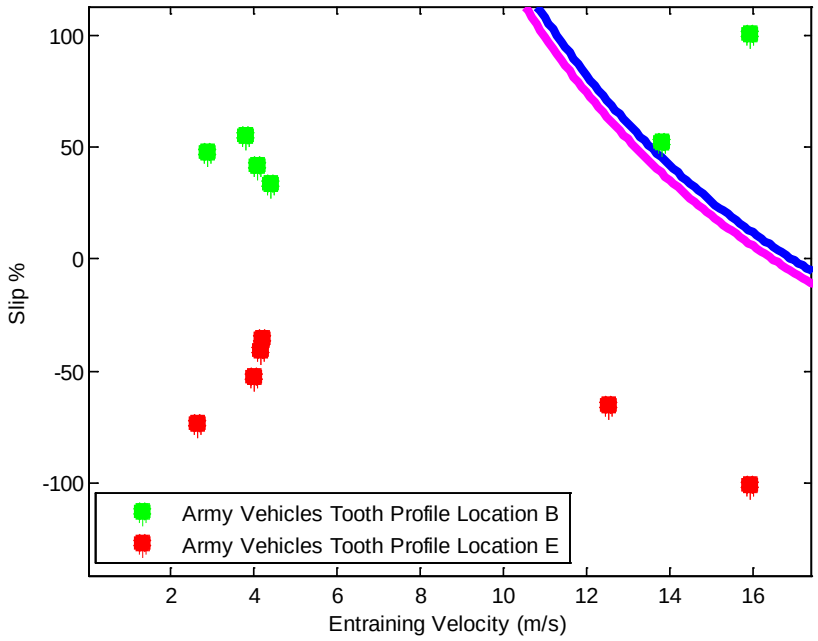

Fig. 19 Contact speeds vs. WAM speed envelope zoomed in

9. Summary and Conclusions

The WAM is a ball-on-disc tribometer used to simulate gear and bearing contacts. The WAM uses independent and bidirectional motors to create a wide variety of entrainment velocities and slip percentages while simultaneously controlling the load to create contact stresses. Its speed envelope and contact stress capabilities were calculated and recorded to inform researchers of the machine's full capabilities. These capabilities are coupled with the knowledge of Army helicopter gear contacts to identify areas where the WAM can fully simulate gear contacts at a coupon level to develop methods for sustaining severe flight conditions. The gear contact conditions can be analyzed under a wide variety of conditions with a wide variety of materials and lubricants to investigate solutions for issues such as reduction in wear or loss of lubrication.

10. References

1. Hamrock BJ, Schmid SR, Jacobson BO. Fundamentals of fluid film lubrication. 2nd edition. New York (NY): CRC Press; 2004.

2. Jackson RL. Lubrication. In: Bruce RW, editor. Handbook of lubrication and tribology. Volume II: theory and design. 2nd ed. Boca Raton (FL): CRC Press; 2012. p. 14-1 through 14-14.

3. Hamrock BJ, Dowson D. Isothermal elastohydrodynamic lubrication of point contacts: part III—fully flooded results. Journal of Tribology.1977;99(2):264–275.

4. Basu B, Kalin M. Tribology of ceramics and composites: a materials science perspective. Hoboken (NJ): John Wiley & Sons; 2011.

5. Deters L. Tribology. In: Grote K-H, Antonsson, EK, editors. Springer handbook of mechanical engineering. New Delhi (India): Springer-Verlag; 2009. p. 295–326.

6. MIL-PRF-23699G. Performance specification, lubricating oil, aircraft turbine engine, synthetic base. Lakehurst (NJ): Naval Air Warfare Center Aircraft Division (US); 2014 Mar 13.

7. SAE J2360. Surface vehicle standard, automotive gear lubricants for commercial and military use. Warrendale (PA): SAE International; 2012 Apr 25.

8. MIL-PRF-2105E. Performance specification, lubricating oil, gear, multipurpose. Warren (MI): Army Tank-Automotive and Armaments Command (US); 1995 Aug 22.

9. AGMA 908-B89. Geometry factors for determining the pitting resistance and bending strength of spur, helical and herringbone gear teeth. Alexandria (VA): American Gear Manufacturers Association; 1989 Apr.

10. Coy JJ, Townsend DP, Zaretsky EV. Gearing. Cleveland (OH): Lewis Research Center, National Aeronautics and Space Administration; 1985 Dec. Report No. NASA RP-1152, AVSCOM TR 84-C-15.

11. ASTM G40-13. Standard terminology relating to wear and erosion. West Conshohocken (PA): ASTM International; 2012 May 1.

12. Davis JR, editor. Gear materials, properties, and manufacture. Materials Park (OH): ASM International; 2005 Sep.

13. Handschuh RF. Gear lubrication. In: Bruce RW, editor. Handbook of lubrication and tribology. Volume II theory and design. 2nd ed. Boca Raton (FL): CRC Press; 2012. p. 50-1 through 50-18.

14. Shigley JE, Mischke CR. Mechanical engineering design. 5th ed. New York (NY): McGraw-Hill Inc.; 1989.

15. Weden G, J Coy, JJ. Summary of drive-train component technology in helicopters. Cleveland (OH): Lewis Research Center, National Aeronautics and Space Administration; 1984. Report No. NASA TM-83726, USAAVSCOM-TR-84-C-10.

16. Holmes M, Evans H, Snidle R. Analysis of mixed lubrication effects in simulated gear tooth contacts. ASME J Tribol. 2005;127(1):61–69.

17. Valco M. Planetary gear train ring gear and support structure investigation [PhD thesis]. [Cleveland (OH)]: Cleveland State University; 1992.

Appendix. Gear Meshing Information

This appendix contains tables of gear meshing information for the OH-58, CH-47, UH-60, and AH-64 helicopters, as well as spur gear specimens in common use at the NASA Glenn Research Center. They have been reproduced with permission, after their original publication by Valco.[1] Five values are given for the sliding velocity, entrainment velocity, and slide-to-roll ratio (SRR). These correspond to points B, C, P, D, and E along the sun tooth.

Table A-1 OH-58D gear meshing data

OH-58D					
Designation	**Light Observation**				
	Sun Gear	**Planet Gear**		**Ring Gear**	
Number of teeth	27	35		99	
Module	2.87	2.87		2.78	
Pressure angle (°)	24.60	24.60		20.19	
Base circle diameter (mm)	70.40	91.26		258.13	
Pitch diameter (mm)	77.43	100.37		275.03	
Root diameter (mm)	70.76	91.54		284.15	
Outside (internal) diameter (mm)	84.05	104.98		–271.75	
Fillet radius (approximate) (mm)	1.27	0.97		1.40	
Backlash with mate (mm)	0.32	. . .		0.24	
Face width (mm)	34.93	31.78		25.40	
Rotor speed (rpm)	. . .	395		. . .	
Gearbox power rating (kW)	. . .	273		. . .	
Planetary reduction ratio	. . .	4.67		. . .	
Gear speed (rpm)	1,844	(722.55)		395	
Spiral bevel reduction ratio	19/71				
Number of planets	. . .	4		. . .	
Helix angle	0	0		0	
Sun/Planet Interaction					
Sliding velocity (m/s)	1.3796	0.5147	0	–1.0846	–1.9495
Entrainment velocity (m/s)	2.8763	2.8205	2.7873	2.7173	2.6615
SRR	0.4796	0.1825	0	–0.3991	–0.7325
Contact stress at pitch point (GPa)	1.35				

[1]Valco M. Planetary gear train ring gear and support structure investigation [PhD thesis]. [Cleveland (OH)]: Cleveland State University, 1992.

Table A-2 CH-47 (lower stage) gear meshing data

CH-47 (Lower Stage)					
Designation	**Heavy Lift**				
	Sun Gear	**Planet Gear**			**Ring Gear**
Number of teeth	28	39			106
Module	5.35	5.35			5.35
Pressure angle (°)	25	25			25
Base circle diameter (mm)	135.7	189.0			513.7
Pitch diameter (mm)	149.7	208.5			566.8
Root diameter (mm)	135.6	194.4			580.1
Outside (internal) diameter (mm)	161.6	218.8			–557.1
Fillet radius (approximate) (mm)	1.7	1.5			1.4
Backlash with mate (mm)	0.6	. . .			0.3
Face width (mm)	48.8	46.1			37.1
Rotor speed (rpm)	. . .	N.A			. . .
Gearbox power rating (kW)	. . .	2813			. . .
Planetary reduction ratio	. . .	4.786			. . .
Gear speed (rpm)	3930	–1411			821
Number of planets	. . .	4			. . .
Sun/Planet Interaction					
Sliding velocity (m/s)	7.2449	2.5547	0	–3.5195	–8.2097
Entrainment velocity (m/s)	13.8115	13.4264	13.2167	12.9278	12.5427
SRR	0.5246	0.1903	0	–0.2722	–0.6545
Contact stress at pitch point (GPa)	1.3				

CH-47 (Upper Stage)					
Designation	**Heavy Lift**				
	Sun Gear	**Planet Gear**			**Ring Gear**
Number of teeth	40	33			106
Module	5.35	5.35			5.35
Pressure angle (°)	25	25			25
Base circle diameter (mm)	193.9	159.9			513.7
Pitch diameter (mm)	213.9	176.5			566.8
Root diameter (mm)	199.8	162.3			580.1
Outside (internal) diameter (mm)	224.7	187.3			–557.1
Fillet radius (approximate) (mm)	1.5	1.6			1.4
Backlash with mate (mm)	0.3	. . .			0.3
Face width (mm)	98.0	101.8			79.0
Rotor speed (rpm)	. . .	225			. . .
Gearbox power rating (hp)	. . .	2813			. . .
Planetary reduction ratio	. . .	3.650			. . .
Gear speed (rpm)	821	–498			225
Number of planets	. . .	6			. . .
Sun/Planet Interaction					
Sliding velocity (m/s)	2.1056	0.7756	0	–0.7901	–2.1200
Entrainment velocity (m/s)	3.8147	3.8785	3.9156	3.9535	4.0173
SRR	0.5520	0.2000	0	–0.1998	–0.5277
Contact stress at pitch point (GPa)	1.3				

Table A-3 UH-60 gear meshing data

UH-60					
Designation	**Utility**				
	Sun Gear	**Planet Gear**		**Ring Gear**	
Number of teeth	62	83		228	
Module	2.87	2.87		2.87	
Pressure angle (°)	22.5	22.5		22.5	
Base circle diameter (mm)	164.27	219.91		604.08	
Pitch diameter (mm)	177.80	238.03		653.86	
Root diameter (mm)	170.88	230.73		661.21	
Outside (internal) diameter (mm)	183.47	243.70		–648.18	
Fillet radius (approximate) (mm)	1.40	1.20		1.22	
Backlash with mate (mm)	0.10	. . .		0.10	
Face width (mm)	81.53	75.44		60.45	
Rotor speed (rpm)	. . .	258		. . .	
Gearbox power rating (kW)	. . .	1,697		. . .	
Planetary reduction ratio	. . .	4.68		. . .	
Gear speed (rpm)	1,207	(450.81)		258	
Number of planets	. . .	5		. . .	
Sun/Planet Interaction					
Sliding velocity (m/s)	1.4982	0.3579	0	–0.3398	–1.4800
Entrainment velocity (m/s)	4.4234	4.3408	4.3149	4.2903	4.2078
SRR	0.3387	0.0825	0	–0.0792	–0.3517
Contact stress at pitch point (GPa)	1.09				

Table A-4 AH-64 gear meshing data

AH-64					
Designation	**Sun Gear**		**Attack Planet Gear**		**Ring Gear**
Number of teeth	48		43		138
Module	3.46		3.46		3.31
Pressure angle (°)	24.9512		24.9512		18.8227
Base circle diameter (mm)	150.52		134.84		432.75
Pitch diameter (mm)	166.02		148.72		457.20
Root diameter (mm)	157.00		138.99		471.20
Outside (internal) diameter (mm)	172.72		155.45		–456.69
Fillet radius (approximate) (mm)	1.09		1.45		1.60
Backlash with mate (mm)	0.32		. . .		0.27
Face width (mm)	60.71		57.15		50.74
Rotor speed (rpm)	. . .		289		. . .
Gearbox power rating (kW)	. . .		1,697		. . .
Planetary reduction ratio	. . .		3.88		. . .
Gear speed (rpm)	1,120		(638.56)		289
Number of planets	. . .		6		. . .
Sun/Planet Interaction					
Sliding velocity (m/s)	1.7176	0.7298	0	–0.7277	–1.7155
Entrainment velocity (m/s)	4.1006	4.1278	4.1478	4.1678	4.1949
SRR	0.4189	0.1768	0	–0.1746	–0.4089
Contact stress at pitch point (GPa)			1.3		

Table A-5 NASA test gears

NASA Test Gears					
Designation	**Spur Gear**				
Number of teeth	28				
Module	6.35				
Pressure angle (°)	20				
Base circle diameter (mm)	167.08				
Pitch diameter (mm)	177.80				
Root diameter (mm)	159.77				
Outside (internal) diameter (mm)	190.50				
Fillet radius (approximate) (mm)	1.27				
Backlash with mate (mm)	0.25				
Face width (mm)	6.35				
Power (kW)	68.25				
Rotation speed (rpm)	1.00E+05				
Sliding velocity (m/s)	16.0777	3.5531	0	–3.5531	–16.0777
Entrainment velocity (m/s)	15.9203	15.9203	15.9203	15.9203	15.9203
SRR	1.0099	0.2232	0	–0.2232	–1.0099
Contact stress at pitch point (GPa)	1.3				

1 (PDF) DEFENSE TECHNICAL INFORMATION CTR DTIC OCA

2 (PDF) DIRECTOR US ARMY RESEARCH LAB RDRL CIO LL IMAL HRA MAIL & RECORDS MGMT

1 (PDF) GOVT PRINTG OFC A MALHOTRA

4 (PDF) DIR USARL RDRL VTP M RIGGS S BERKEBILE A HOOD B DYKAS

INTENTIONALLY LEFT BLANK.